Available online at www.sciencedirect.com

ScienceDirect

Proceedings of the Combustion Institute 37 (2019) 885–892

Proceedings of the Combustion Institute

www.elsevier.com/locate/proci

Insights into incipient soot formation by atomic force microscopy

Fabian Schulz [a,1], Mario Commodo [b,1], Katharina Kaiser [a], Gianluigi De Falco [c], Patrizia Minutolo [b], Gerhard Meyer [a], Andrea D'Anna [c,*], Leo Gross [a,*]

[a] *IBM Research – Zurich, Säumerstrasse 4, 8803 Rüschlikon, Switzerland*
[b] *Istituto di Ricerche sulla Combustione, CNR, P.le Tecchio 80, 80125 Napoli, Italy*
[c] *Dipartimento di Ingegneria Chimica, dei Materiali e della Produzione Industriale - Università degli Studi di Napoli Federico II, P.le Tecchio 80, 80125 Napoli, Italy*

Received 30 November 2017; accepted 13 June 2018
Available online 3 July 2018

Abstract

Combustion-generated soot particles can have significant impact on climate, environment and human health. Thus, understanding the processes governing the formation of soot particles in combustion is a topic of ongoing research. In this study, high-resolution atomic force microscopy (AFM) was used for direct imaging of the building blocks forming the particles in the early stages of soot formation. Incipient soot particles were collected right after the particle nucleation zone of a slightly sooting ethylene/air laminar premixed flame at atmospheric pressure and analyzed by AFM after a rapid sublimation procedure. Our data shed light on one of the most complex and still debated aspect on soot formation, i.e., the nucleation process. The molecular constituents of the initial particles have been individually analyzed in detail in their chemical/structural characteristics. Our data demonstrate the large complexity/variety of the aromatic compounds which are the building blocks of the initial soot particles. Nevertheless, some fundamental and specific characteristics have been clearly ascertained. These include a significant presence of penta-rings as opposed to the purely benzenoid aromatic compounds and the noticeable presence of aliphatic side-chains. In addition, there were indications for the presence of persistent π radicals. Incipient soot was also investigated by Raman spectroscopy, the results of which agreed in terms of chemical and structural composition of the particles with those obtained by AFM.

Keywords: Incipient soot; Nucleation; Atomic force microscopy; Atomic resolution; Raman spectroscopy

* Corresponding authors.
E-mail addresses: anddanna@unina.it (A. D'Anna), lgr@zurich.ibm.com (L. Gross).
[1] These authors contributed equally.

https://doi.org/10.1016/j.proci.2018.06.100
1540-7489

1. Introduction

Soot formation in combustion is a topic of great relevance because of the adverse implications on the human health and on the environment. Soot particles are known to be harmful, particularly when their size is at the nanoscale, having numerous and ascertained negative health effects [1–3]. In addition, the emission of soot in the atmosphere has complex implications in affecting the environment and particularly the climate change [4]. Therefore, the need to reduce the emission of these carbon nanoparticles into the atmosphere pushes for a better understanding of the chemical and physical mechanisms behind the soot formation process. However, understanding soot formation in combustion is not a trivial task. Soot formation/evolution chemistry, in fact, is a complex process involving gas-phase fuel-rich flame chemistry, gas-to-particle transition, particle coagulation and/or coalescence, heterogeneous growth, particle agglomeration, carbonization and oxidation. Among all, it is quite certain that the most complex, yet unresolved and scientifically intriguing phenomenon is the nucleation [5–8]. It is well known that polycyclic aromatic hydrocarbons (PAHs) are key compounds acting as building blocks. However, many aspects are still under debate and object of ongoing experimental and theoretical studies. These include: size [9], chemical composition, e.g., presence of heteroatoms and in particular of oxygen atoms [10], presence of penta-rings [11], as well as cross-linking among two or several aromatic groups [12,13] and aliphatic side chains [14]. Once formed, these aromatic structures begin to assemble into just-nucleated particles or clusters, whose size is usually of the order of few nanometers, i.e., 2–3 nm [5–8]. Two distinct clustering processes have been hypothesized over the years and often referred to as physical and chemical pathways. The former considers the soot nucleation/clustering process as a homogeneous condensation process purely due to the occurrence of physical van der Waals attractive forces between aromatic molecules, which are commonly assumed in soot models to be pyrene or slightly larger *peri*-condensed PAHs. By contrast, the latter considers soot inception as proceeding through the formation of chemical bonds connecting two or more aromatics to form polymer-like assemblies and/or macromolecules [5].

To date, most of the data on incipient soot molecular/chemical composition derive from mass spectrometric studies [15–18] and optical/spectroscopic methods [19–23]. Unfortunately, the former has limited capability in providing detailed information or molecular assignment as the mass of the molecule increases, and the latter yields only global chemical/structural information for such complex ensembles of chemical compounds. To better understand the chemical composition of precursor particles it is necessary to use analytical methods capable of providing more detailed information on the molecular structure of the aromatic building blocks forming the incipient soot particles.

Scanning probe microscopy (e.g., scanning tunneling microscopy, STM and atomic force microscopy, AFM) is uniquely capable to image adsorbates at the atomic scale. In particular, it is possible to image single molecules with atomic resolution using AFM [24]. This major advancement is enabled by using atomically functionalized tips, which probe the repulsive forces above single molecules [25]. Consequently, this method was also applied to measure bond order [26], identify the atomic structure of natural compounds [27] as well as the constituents of complex molecular mixtures [28,29] and follow the intermediate steps of on-surface reactions [30,31].

Complementary to AFM, STM gives access to electronic properties of adsorbates. When using an ultrathin insulating layer as substrate, STM can be used, e.g., to map molecular orbital densities [32–34]. The combination of these two techniques provides a powerful tool to identify the chemical structure of unknown molecules [28].

In this work, incipient soot nanoparticles generated in a laminar premixed ethylene/air flame have been decomposed into their molecular constituent building blocks and investigated by high-resolution AFM. These measurements yield important and unique information on the types and chemical characteristics of the aromatic building blocks forming the just-incepted particles. In addition, sampled incipient particles have also been investigated by Raman spectroscopy. The findings obtained from the whole set of analysis constitute an important step forward in the understanding of the chemistry of the soot particles at the early stage of their formation, thus contributing to the foundation and guidance of future detailed soot models.

2. Experimental

An atmospheric-pressure laminar premixed ethylene–air flame was stabilized on a McKenna burner having a diameter of 6 cm. The cold gas velocity was set at 9.8 cm/s and carbon to oxygen (C/O) atomic ratio fixed at 0.67, i.e., equivalence ratio $\Phi = 2.03$. The accurate setting of the combustion parameters ensured long-term stability of gas-flow velocity, composition and flame temperature.

Incipient soot particles were collected from the flame at a height above the burner (HAB) of 8 mm. The combustion products were extracted from the flame centerline by means of a high-dilution horizontal tubular probe [35]. Specifically, the combustion products were sampled through a very small orifice, i.e., 200 μm, located on the bottom side of the probe and rapidly mixed with N_2, thus

providing a dilution ratio of 1:($3{\cdot}10^3$) [36]. This sampling procedure prevents particles from coagulating, and allows quenching the chemical reactions throughout the sampling line [35]. Flame temperature profiles, with and without probe, have been reported elsewhere [36]. The particle size distribution (PSD) was measured on-line using a differential mobility analyzer (DMA) system composed by an electrostatic aerosol classifier Vienna–type DMA (TapCon 3/150, size range of 1–40 nm), an X-ray diffusion charging source (TSI Mod. 3088), and a Faraday cup electrometer. For the off-line analyses, a stainless-steel aerosol filter holder containing a quartz filter (Whatman QMA grade, 47 mm) was positioned on-line downstream of the dilution tubular probe for soot nanoparticles collection. Gas temperature at the filter location was 350 K. At this temperature and in the high dilution condition, the condensation of gas-phase PAHs should be disfavored up to the size of ovalene. The sample collection lasted 14 hours to gather enough material on the filter for off-line analysis. The flame temperature was monitored and found to be constant within ± 10 °C during the sampling time. Preliminary control experiments on the sampling procedure/reproducibility were performed by Raman spectroscopy.

STM and AFM measurements were carried out in a home-built combined STM/AFM set–up operated at low temperature ($T \approx 5$ K) and ultra-high vacuum (UHV, $p \approx 1 \times 10^{-10}$ mbar). The microscope was equipped with a qPlus quartz cantilever [37] operated in the frequency modulation mode [38] (resonance frequency $f_0 \approx 28.8$ kHz, spring constant $k \approx 1.8$ kN/m, quality factor $Q \approx 100{,}000$ and oscillation amplitude $A \approx 0.6$ Å). The bias voltage was applied to the sample and STM images were taken in the constant-current mode. AFM images were taken in the constant-height mode and at 0 V bias voltage. Positive height offsets, z, correspond to a decrease of the tip-sample distance with respect to the STM set-point. A Cu(111) single crystal partially covered with (100)-oriented, two monolayer (ML) thick NaCl islands [denoted as NaCl(2ML)/Cu(111)] was used as substrate. The Cu(111) crystal was cleaned by repeated cycles of Ne^+ sputtering and annealing to ~800 K. Subsequently, NaCl was evaporated onto the clean Cu(111) surface at ~ 270 K. Small amounts of carbon monoxide (CO) were dosed onto the surface at ~10 K for tip functionalization by admitting CO into the UHV chamber. The microscope tip was made from 25 μm-thick PtIr wire sharpened with a focused ion beam. A clean and sharp Cu tip was prepared *in situ* by deliberate indentations into the Cu(111) substrate. The tip apex was passivated by picking up a single CO molecule from the surface [39].

The soot nanoparticles were deposited onto the substrate by applying a small amount of material from the quartz filter onto a piece of silicon wafer by gently pressing the filter onto the wafer. The wafer was subsequently introduced into the UHV system and flash-heated by resistive heating to evaporate the molecules onto the cold sample ($T \approx 10$ K). Thereby, the wafer was heated from room temperature to ~900 K within a few seconds. We have previously carried out several control experiments concerning reproducibility, reliability and statistical significance of this preparation method [29,40]. PAHs including archipelago-type molecules with masses up to about 600 Da [40] sublime intact from the silicon wafer. Thus, molecular mixtures containing molecules with masses below 600 Da will be deposited without significant changes in composition and structure on the surface. This has been corroborated by comparison of AFM data on mixtures with mass spectroscopy data [29]. For the sample of nascent soot investigated in this study, showing mean masses on the order of 350 Da and only a very small part of molecules > 600 Da, the flash-heating method is suitable.

STM/AFM experiments were performed within a few days after sampling. We are confident that the sample does not undergo significant chemical/structural modification during such time period as corroborated by the reproducibility of the Raman and light absorption spectra of the sample over several days. We also did not observe isomerization or decomposition of the imaged molecules during STM/AFM characterization.

Raman spectroscopy was performed by positioning the filter without further manipulation under the microscope (Horiba XploRA) equipped with a 100X objective (NA0.9 Olympus), a Nd:YAG laser ($\lambda = 532$ nm, 12 mW maximum laser power at the sample) and a 200 μm pinhole for confocal photons collection. System calibration was performed against the Stokes Raman signal of pure silicon at 520 cm^{-1}. A. The power of the excitation laser beam was attenuated to 1% to avoid structural changes of the sample due to thermal decomposition when using an accumulation-exposure time of 5 cycles of 30 s each. A total of 10 spots were randomly selected to verify the homogeneity of the sample and finally averaged to obtain a statistically relevant Raman spectrum. The standard deviation was of the order of few percent.

3. Results and discussion

The whole set of experiments was conducted on incipient soot particles collected from a laminar premixed flame at a fixed C/O ratio and distance from the burner exit, i.e., C/O = 0.67 and HAB = 8 mm. In this flame condition, particles presented a unimodal PSD with a maximum positioned between 2 and 2.5 nm (mobility diameter), as shown in Fig. 1.

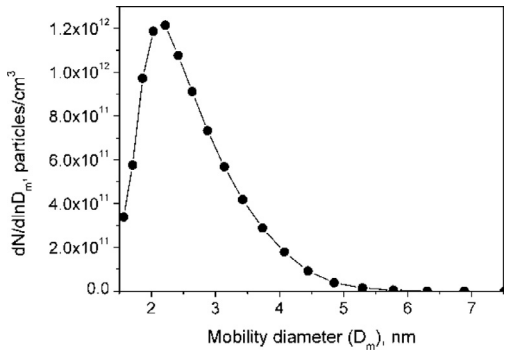

Fig. 1. Particle size distribution at 8 mm above the burner of the laminar premixed flame measured by DMA.

This particle mode is well representative of the onset of soot formation as also described in a previous work [36]. Only at higher residence times, i.e., at increased HABs, the particle growth process due to coagulation/coalescence and surface mass addition was evidenced from the formation of a second mode centered at larger diameters in the PSD, which clearly appeared as bimodal [36].

The particles collected on the quartz filter were subsequently investigated by low-temperature atomic-resolution AFM/STM, and Raman spectroscopy.

A typical STM overview image of the NaCl(2ML)/Cu(111) substrate after sublimation of soot nanoparticles is shown in the left panel of Fig. 2. Located on the bottom part is a NaCl(2ML) island, and several CO molecules and sublimated soot particles are adsorbed on the surface. Importantly, due to the particle deposition *via* flash–heating, any clusters potentially formed by van der Waals stacking during the nucleation process are expected to break down into its aromatic building blocks. The right panel of Fig. 2 shows an STM image and two high-resolution AFM images taken at different tip-sample distances for three characteristic compounds found in this study (**M1, M2, M3**), respectively. The AFM images show the carbon skeleton of the PAH cores as repulsive (bright) contrast, which becomes more pronounced as the tip-sample distance is decreased. In addition, the bonds get slightly distorted at closer distances, which is due to the flexibility of the CO at the tip apex [26,41,42]. Comparison with previous AFM studies of reference molecules also enables the assignment of methyl groups [28], aliphatic moieties [40] and oxygen-containing side groups such as ketones [43] and methoxy groups [27]. The proposed chemical structures of **M1, M2**, and **M3** are shown next to the AFM images in Fig. 2. Specifically, the compound **M1** ($C_{24}H_{12}$) is made of a central *peri*-condensed aromatic core composed by six fused benzene rings and one additional five-membered ring on the periphery of the molecule.

Compounds **M2** ($C_{31}H_{16}$) and **M3** ($C_{44}H_{20}$) show a larger conjugation length, i.e., a higher number of fused benzene rings, containing 9 and 13 benzene rings, respectively. **M3** also contains two penta-rings, similar to **M1**. Indeed, our study reveals that such peripheral five-membered rings are a common motif in the molecular constituents of incipient soot nanoparticles. However, in contrast to **M1**, the two penta-rings in **M3** are not fully aromatic. Their two outer carbon atoms are sp^3 hybridized and doubly hydrogenated, thus forming cycloaliphatic moieties [40]. This causes their bright contrast in the AFM images and the distortions at close tip-sample distance. Interestingly,

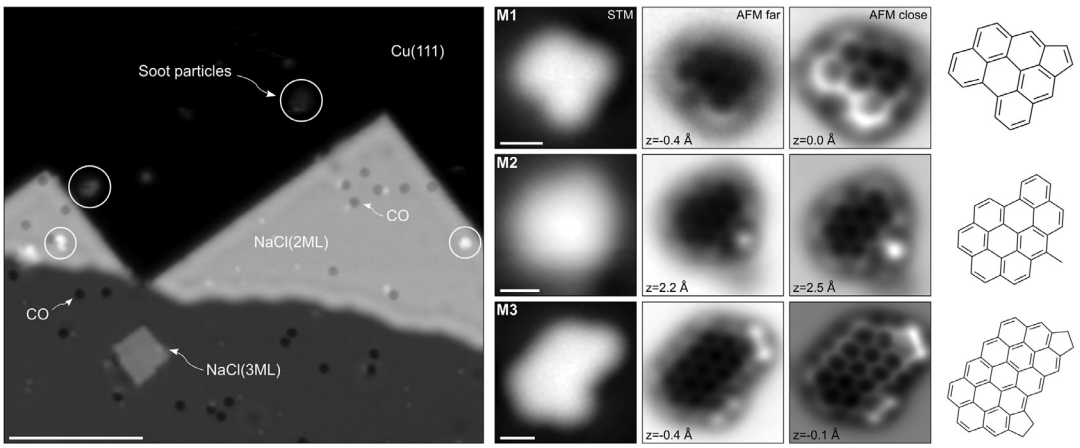

Fig. 2. Left panel: STM overview image ($I = 0.5$ pA, $V = 0.4$ V) of the sample after deposition of soot particles. Scale bar is 10 nm. Right panel: STM and AFM images of molecules **M1** [on NaCl(2ML)/Cu(111)], **M2** [on Cu(111)] and **M3** [on NaCl(2ML)/Cu(111)] at different set-points z from ($I = 0.5$ pA, $V = 0.2$ V). Scale bars are 5 Å.

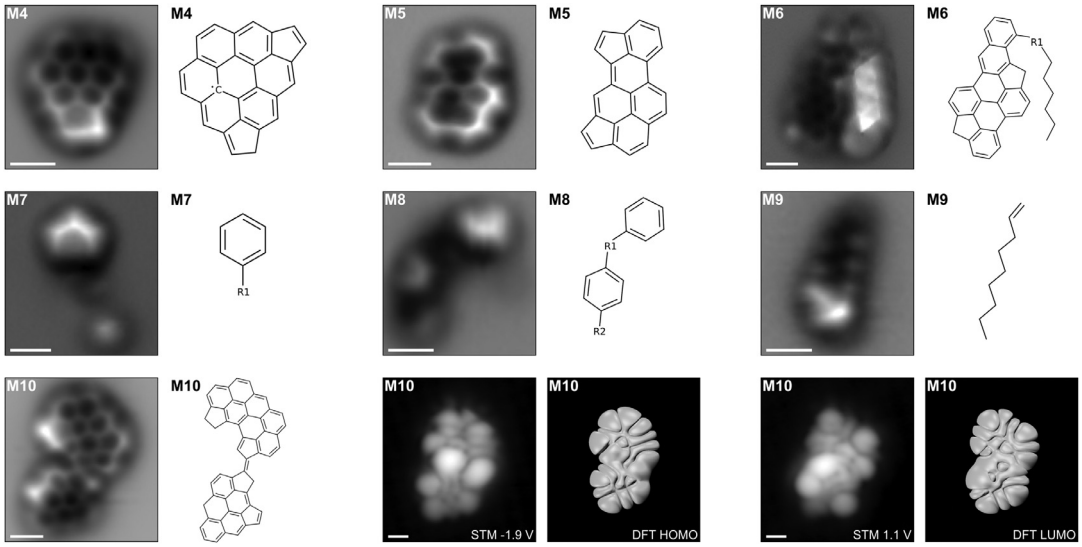

Fig. 3. AFM images and chemical structure of some representative molecules, as well as molecular orbital densities measured by STM for **M10** and corresponding DFT simulations. "*R*" labels denote unidentified parts of the molecules. Scale bars are 5 Å.

another aliphatic moiety can be identified in compound **M2,** which contains a side group attributed to a methyl (–CH_3). The presence of aliphatic contributions in just-nucleated soot particles was reported in previous studies [18–20,23]. However, to the best of our knowledge, our data represent the first direct observation of aliphatic-substituted aromatics in soot particles.

The aim of this work is to characterize common molecular structures and motives in early soot formation by atomic-resolution AFM. However, a statistical analysis and quantification of the compounds goes beyond the scope of this work. A comparison with mass spectrometry indicated the statistical significance of the sampling by AFM [29]. However, quantification in complex mixtures by AFM remains extremely challenging because of the large number of molecules that need to be imaged and because all molecules in sampling areas should be assigned. Here, we focus our analysis on planar PAHs and aliphatic chains, which permit reliable chemical structure assignment by AFM. Such molecules made up about half of the adsorbates found on the sample surface after preparation. The other half of the molecules were too non-planar and/or very mobile under the influence of the tip and for that reasons could not be imaged with atomic resolution.

A detailed discussion of the entire set of measured molecules and their assigned structure would be out of scope of this article and will be provided in a separate manuscript. Instead, we report in Fig. 3 further selected structures which represent the different groups of molecules observed during the STM/AFM measurements. Molecule **M4** ($C_{28}H_{13}$), for example, is composed of seven fused benzene rings, i.e., coronene, and two additional five–membered rings on the periphery of the molecule. Because one of the penta-rings contains a doubly-hydrogenated carbon, this compound represents one of the few cases where the assigned structure suggests the presence of an aromatic radical. However, the assignment of the in part aliphatic penta-rings is tentative and needs to be corroborated further by the measurement of known standards. The role of aromatic π radicals, and particularly the contribution of radical sites as active sites for carbon addition has long being hypothesized in the soot formation process [44]. In addition, the relevance of aromatic radicals resulting from localized π electron in the particle nucleation process and during the subsequent mass growth has been recently remarked in Wang's review paper [6].

Molecule **M5** ($C_{24}H_{12}$) contains five fused benzene rings and two penta-rings and is one of the smaller PAH cores found in our study. Interestingly, its shape is more elongated and shows partial *cata*-condensation, while most of the identified structures were purely *peri*-condensed. Compound **M6** represents one of the most complex structures found during the measurements. It contains a PAH core made from seven benzene rings and two penta-rings. In contrast to the previously discussed structures, here the penta-rings are not located at peripheral zigzag regions but embedded in armchair edges. In addition, the outer carbon of both penta-rings is doubly hydrogenated. Finally,

one of the benzene rings is *cata*-condensed at the periphery and further connected to a long, aliphatic side group. This chain can be identified as an alkyl chain [$(CH_2)_n$], based on the very bright contrast in the AFM image and its characteristic modulation [40].

Compounds with low conjugation length together with some purely aliphatic ones were also observed, e.g., **M7, M8**, and **M9**. These molecules included: substituted benzene molecules, e.g., compound **M7**; aliphatic-linked aromatic compounds, e.g., **M8**; and some isolated aliphatic chains, e.g., **M9**. In **M8**, both six-membered rings are tilted out of the surface plane, indicating sterical hindrance due to the attached side groups.

On the other hand, **M10** ($C_{52}H_{26}$; 650.76 u; $H/C = 0.5$) is one of the largest identified compounds. Interestingly, although the majority of imaged soot fragments were in the form of "*singlet*" isolated PAHs, the structure of **M10** suggests the covalent linking of two aromatic "*islands*". To confirm the assigned molecular structure of **M10**, its highest occupied (HOMO) and lowest unoccupied (LUMO) molecular orbital densities were measured by STM, the results being shown in Fig. 3 along with **M10**. These were compared to *ab initio* electronic structure calculations using the assigned chemical structure as input. For the calculations, we employed density functional theory (DFT) with the PBE exchange-correlation functional [45], as implemented in the FHI-aims code [46]. The HOMO and LUMO calculated from DFT are shown in Fig. 3 next to the measured orbital densities. The agreement is excellent, thus confirming our assigned structure. Importantly, **M10** represents the first experimental evidence of so-called "*archipelago*" compounds within the pool of molecules participating in the soot formation.

It is worth noticing that most of the observed penta-rings are positioned mainly on the zigzag region of the hexagonal aromatic structure. This is consistent with their formation by addition of one acetylene molecule and subsequent ring closure [47]. By contrast, bowl-shaped PAHs containing five-membered ring surrounded by hexagons, such as corannulene ($C_{20}H_{10}$) or similar aromatics, were rarely observed.

In general, we observed that the majority of the carbon atoms on the periphery of the aromatic molecules were either in "*zigzag*" or "*armchair*" conformation, while "*cove*" are very rare and "*fjord*" types [48] were never observed.

Recent literature also reports a contribution of oxygenated compounds in the formation of soot particles both in diffusion [18] and premixed flame conditions [9,49]. In the current study, none of the molecules identified by AFM presented clear evidence of oxygens incorporated into the PAH core or as ketones. However, oxygen could be contained in non-planar fragments and bulky side groups, which are challenging to characterize with AFM.

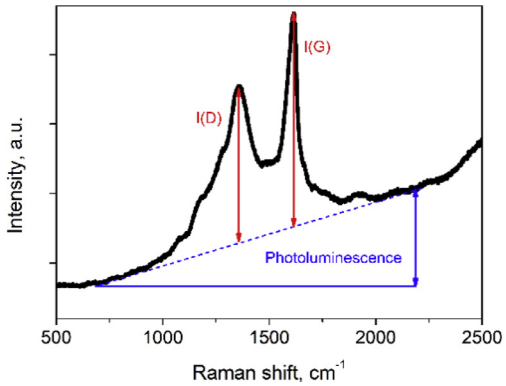

Fig. 4. Raman spectrum of incipient soot nanoparticles.

Just-nucleated soot particles were also investigated by Raman spectroscopy. This spectroscopic technique is known to be an excellent tool for collecting detailed information about the electronic and chemical structure of any carbon-based material, including amorphous carbon [50]. In recent years, Raman spectroscopy has also become a common analytical method for soot micro/nanostructure investigations [51–53].

The first-order Raman spectrum, 1000–1800 cm^{-1}, of the sample is reported in Fig. 4. It presents two main features, i.e., the G and D peak, which normally dominate in the Raman spectrum of any disordered carbonaceous materials [50]. The ability of Raman spectroscopy to probe chemical/structural information of carbon materials lies in the fact that the presence of defects in the sp^2 aromatic network allows the activation of the Raman D mode at ~1350 cm^{-1}, prohibited in the perfect hexagonal lattice. Edge effects in small graphitic domains are one major source of this band. Conversely, the G band, at ~1600 cm^{-1}, due to every sp^2 carbon, is mostly insensitive to defects and only presents small changes in width and position of the maximum as function of the different carbon structures [50]. Besides these two bands, other interesting features can be observed in the spectrum of Fig. 4. These include a relevant signal in the valley region between the D and G band and some defined bumps in the spectral region 1000–1250 cm^{-1}. For disordered carbon materials and soot, various assignments have been proposed for such features [50,51,54]. Ferrari and Robertson [50] attributed the peak at 1150 cm^{-1} to trans-polyacetylene. The presence of aliphatic chains in incipient soot are clearly demonstrated by the AFM results reported here, e.g., soot fragment **M9** or the side-group in **M6**. However, the observed aliphatic chains are mainly alkyl chains,

i.e., polyethylene, which also present vibration in this spectral range [55]. Such chains, together with the five-membered rings, may also be responsible for the signal in the intra-valley region at about 1500 cm^{-1}.

Importantly, it is well recognized that the relative intensity of the D and G peak, $I(D)/I(G)$, can be expressed as function of the size of graphitic domains, L_a [50].

Particularly, in the case of highly disordered/amorphous carbon materials, i.e., for very small size of the graphite crystallites such as the case of flame-formed soot particles [52,53], the following empirical expression has been found to correlate L_a with the relative intensity of the two Raman peaks [50]:

$$L_a^2(\mathrm{nm}^2) = 5.4 \cdot 10^{-2} \cdot E_L^4(\mathrm{eV}^4)\frac{I(D)}{I(G)} \quad (1)$$

where E_L is the energy of the incident photon. From the measured Raman spectra, we obtain a $I(D)/I(G)$ value of 0.76 ± 0.02, which results in $L_a = 1.1$ nm using Eq. (1). This value of L_a, roughly corresponding to the size of ovalene, agrees reasonably well with the average size of the aromatic building blocks imaged by AFM. A similar size of the aromatic constituents of incipient soot has been previously reported using optical band gap analysis [36,56] and HR-TEM [56,57].

Furthermore, from the analysis of the photoluminescence background in the Raman spectrum, see Fig. 4, we can also obtain additional chemical information on the nascent soot particles. Casiraghi et al. [58] found an empirical equation that can be used for determining the hydrogen to carbon atomic ratio for hydrogenated amorphous carbon based on the measured ratio between the slope of the photoluminescence background of the Raman spectrum, m, and the intensity of the G band, $I(G)$:

$$H[at.\%] = 21.7 + 16.6 * \log\left\{\frac{m}{I(G)}[\mu\mathrm{m}]\right\} \quad (2)$$

where H[at%] is the atomic percentage of hydrogen from which it is possible to calculate the H/C ratio. From the measured Raman spectra, we obtained $m/I(D) = 3.2 \pm 0.5$ that gives, by using Eq. (2), an average H/C value of 0.43 ± 0.03, which is to a good extent consistent with the H/C of the compounds observed by AFM.

Overall, the Raman spectroscopy measurements agree well with the size and structure of the molecules found by STM/AFM. This indicates that the molecular composition of the sample is not altered by the sample preparation process for STM/AFM characterization and that the assigned PAHs are indeed building blocks in early soot formation.

4. Conclusions

Incipient soot nanoparticles generated in a laminar premixed ethylene/air flame were investigated by low-temperature atomic-resolution AFM and Raman spectroscopy. The chemical structure of individual aromatic building blocks contributing to the formation/nucleation of soot particles could be identified, thereby confirming some previous assumptions but also providing novel, important insights:

- AFM data corroborate the large complexity/variety of the aromatic compounds participating in the formation of the initial soot particles.
- Penta-rings were frequently observed in the imaged aromatic molecules.
- Several molecules contained non-aromatic side-groups such as cycloaliphatic moieties, methyl groups and alkyl chains.
- There are indications for the presence of unpaired π–electrons within the aromatic building blocks.
- AFM data present the first experimental evidence of cross-linked aromatic compounds within the pool of molecules participating in the soot formation.
- The average size of aromatics moieties in incipient soot, retrieved by Raman spectroscopy, is of the order of 1.1 nm, with an average H/C ratio of 0.43, thus in good agreement with the AFM observations.

Acknowledgments

We thank R. Allenspach and S. Fatayer for comments and discussions. This work was financially supported by the ERC Consolidator Grant AMSEL (682144) and by Accordo di Programma CNR-MSE Ricerca di Sistema Elettrico – Project "MIcro co/tri generazione di Bioenergia Efficiente e Stabile (Mi-Best)".

References

[1] I.M. Kennedy, *Proc. Combust. Inst.* 31 (2007) 2757–2770.
[2] P. Pedata, T. Stoeger, R. Zimmermann, A. Peters, G. Oberdörster, A. D'Anna, *Part. Fibre Toxicol.* 12 (2015) 34.
[3] G. De Falco, C. Colarusso, M. Terlizzi, et al., *Front. Immunol.* 8 (2017) 1415.
[4] T.C. Bond, S.J. Doherty, D.W. Fahey, et al., *J. Geophys. Res. Atmos.* 118 (2013) 5380–5552.
[5] A. D'Anna, *Proc. Combust. Inst.* 32 (2009) 593–613.
[6] H. Wang, *Proc. Combust. Inst.* 33 (2011) 41–67.
[7] P. Desgroux, X. Mercier, K.A. Thomson, *Proc. Combust. Inst.* 34 (2013) 1713–1738.
[8] H.A. Michelsen, *Proc. Combust. Inst.* 36 (2017) 717–735.

[9] T.S. Totton, A.J. Misquitta, M. Kraft, *Phys. Chem. Chem. Phys.* 14 (2012) 4081–4094.
[10] K.O. Johansson, T. Dillstrom, M. Monti, et al., *Proc. Natl. Acad. Sci. USA* 113 (30) (2016) 8374–8379.
[11] E.K.Y. Yapp, C.G. Wells, J. Akroyd, S. Mosbach, Rong Xu, Markus Kraft, *Combust. Flame* 176 (2017) 172–180.
[12] L. Pascazio, M. Sirignano, A. D'Anna, *Combust. Flame* 185 (2017) 53–62.
[13] A. D'Anna, A. Violi, A. D'Alessio, A.F. Sarofim, *Combust. Flame* 127 (2001) 1995–2003.
[14] P. Elvati, A. Violi, *Proc. Combust. Inst.* 34 (2013) 1837–1843.
[15] R.A. Dobbins, R.A. Fletcher, H.-C. Chang, *Combust. Flame* 115 (1998) 285–298.
[16] B. Apicella, A. Carpentieri, M. Alfe', et al., *Proc. Combust. Inst.* 31 (2007) 547–553.
[17] A. Faccinetto, P. Desgroux, M. Ziskind, E. Therssen, C. Focsa, *Combust. Flame* 158 (2011) 227–239.
[18] J. Cain, A. Laskin, M.R. Kholghy, M.J. Thomson, H. Wang, *Phys. Chem. Chem. Phys.* 16 (2014) 25862.
[19] A. Santamaría, F. Mondragón, A. Molina, N.D. Marsh, E.G. Eddings, A.F. Sarofim, *Combust. Flame* 146 (2006) 52–62.
[20] C. Russo, A. Tregrossi, A. Ciajolo, *Proc. Combust. Inst.* 35 (2015) 1803–1809.
[21] M. Commodo, G. Tessitore, G. De Falco, A. Bruno, P. Minutolo, A. D'Anna, *Proc. Combust. Inst.* 35 (2015) 1795–1802.
[22] E.M. Adkins, J.H. Miller, *Phys. Chem. Chem. Phys.* 17 (2015) 2686.
[23] M. Commodo, A. D'Anna, G. De Falco, R. Larciprete, P. Minutolo, *Combust. Flame* 181 (2017) 188–197.
[24] L. Gross, F. Mohn, N. Moll, P. Liljeroth, G. Meyer, *Science* 325 (2009) 1110–1114.
[25] N. Moll, L. Gross, F. Mohn, A. Curioni, G. Meyer, *New J. Phys.* 14 (2012) 083023.
[26] L. Gross, F. Mohn, N. Moll, et al., *Science* 337 (2012) 1326–1329.
[27] K.Ø. Hanssen, B. Schuler, A.J. Williams, et al., *Angew. Chem. Int. Ed.* 51 (2012) 12238–12241.
[28] B. Schuler, G. Meyer, D. Peña, O.C. Mullins, L. Gross, *J. Am. Chem. Soc.* 137 (2015) 9870–9876.
[29] B. Schuler, S. Fatayer, G. Meyer, et al., *Energy Fuels* 31 (2017) 6856–6861.
[30] D.G. de Oteyza, P. Gorman, Y.-C. Chen, et al., *Science* 340 (2013) 1434–1437.
[31] F. Schulz, P.H. Jacobse, F.F. Canova, et al., *J. Phys. Chem. C* 121 (2017) 2896–2904.
[32] J. Repp, G. Meyer, S.M. Stojković, A. Gourdon, C. Joachim, *Phys. Rev. Lett.* 94 (2005) 026803.
[33] L. Gross, N. Moll, F. Mohn, et al., *Phys. Rev. Lett.* 107 (2011) 086101.
[34] F. Schulz, M. Ijäs, R. Drost, et al., *Nat. Phys.* 11 (2015) 229–234.
[35] B. Zhao, Z. Yang, J. Wang, M.V. Johnston, H. Wang, *Aerosol Sci. Technol.* 37 (2003) 611–620.
[36] M. Commodo, G. De Falco, A. Bruno, C. Borriello, P. Minutolo, A. D'Anna, *Combust. Flame* 162 (2015) 3854–3863.
[37] F.J. Giessibl, *App. Phys. Lett.* 73 (1998) 3956.
[38] T.R. Albrecht, P. Grütter, D. Rugar, *Appl. Phys. Lett.* 69 (1991) 668–673.
[39] L. Bartels, G. Meyer, K.-H. Rieder, *Appl. Phys. Lett.* 71 (1997) 213–215.
[40] B. Schuler, Y. Zhang, S. Collazos, et al., *Chem. Sci.* 8 (2017) 2315–2320.
[41] P. Hapala, G. Kichin, C. Wagner, F.S. Tautz, R. Temirov, P. Jelínek, *Phys. Rev. B* 90 (2014) 085421.
[42] S.K. Hämäläinen, N. van der Heijden, J. van der Lit, S. den Hartog, P. Liljeroth, I. Swart, *Phys. Rev. Lett.* 113 (2014) 186102.
[43] A. Mistry, B. Moreton, B. Schuler, et al., *Chem. Eur. J.* 21 (2015) 2011–2018.
[44] J.B. Howard, *Proc. Combust. Inst.* 23 (1991) 1107–1127.
[45] J.P. Perdew, K. Burke, M. Ernzerhof, *Phys. Rev. Lett.* 77 (1996) 3865–3868.
[46] V. Blum, R. Gehrke, F. Hanke, et al., *Comput. Phys. Commun.* 180 (2009) 2175–2196.
[47] H. Wang, M. Frenklach, *J. Phys. Chem.* 98 (1994) 11465–11489.
[48] F.S. Ehrenhauser, *Polycycl. Aromat. Compd.* 35 (2015) 161–176.
[49] M. Commodo, G. De Falco, R. Larciprete, A. D'Anna, P. Minutolo, *Exp. Therm. Fluid Sci.* 73 (2016) 56–63.
[50] A.C. Ferrari, J. Robertson, Phil. Trans. R. Soc. Lond. *A* 362 (2004) 2477–2512.
[51] J.D. Herdman, B.C. Connelly, M.D. Smooke, M.B. Long, J.H. Miller, *Carbon* 49 (2011) 5298–5311.
[52] P. Minutolo, M. Commodo, A. Santamaria, G. De Falco, A. D'Anna, *Carbon* 68 (2014) 138–148.
[53] M. Commodo, P.H. Joo, G. De Falco, P. Minutolo, A. D'Anna, O.L. Gülder, *Energy Fuels* 31 (2017) 10158–10164.
[54] M.W. Smith, Ian Dallmeyer, T.J. Johnson, et al., *Carbon* 100 (2016) 678–692.
[55] M.J. Gall, P.J. Hendra, O.J. Peacock, M.E.A. Cudby, H.A. Willis, *Spectrochim. Acta A* 28 (1972) 1485–1496.
[56] M.L. Botero, E.M. Adkins, H.Miller S.González-Calera, M. Kraft, *Combust. Flame* 164 (2016) 250–258.
[57] B. Apicella, P. Pré, M. Alfè, et al., *Proc. Combust. Inst.* 35 (2015) 1895–1902.
[58] C. Casiraghi, F. Piazza, A.C. Ferrari, D. Grambole, J. Robertson, *Diam. Relat. Mater.* 14 (2005) 1098–1102.